Velmurugan and Warrier
Journal of Engineering and Applied Science (2022) 69:92
https://doi.org/10.1186/s44147-022-00143-y

Journal of Engineering and Applied Science

RESEARCH Open Access

Production of biodiesel from waste cooking oil using mesoporous MgO-SnO_2 nanocomposite

Amirthavalli Velmurugan[1] and Anita R. Warrier[2*]

*Correspondence: anitawarrier2@gmail.com

[1] Department of Petroleum Engineering, Academy of Maritime Education and Training, Chennai, Tamil Nadu, India
[2] Nanophotonics Research Laboratory, Department of Physics, Academy of Maritime Education and Training, Chennai, Tamil Nadu, India

Abstract

Mesoporous, bifunctional MgO-SnO_2 nanocatalysts with enhanced surface area are used for producing biodiesel from waste cooking oil. Biodiesel with yield of 80% is achieved within the first 20 min when transesterification is carried out at an optimum condition of 18:1 methanol to oil ratio, 2 wt% of nanocatalyst, and at a reaction temperature of 60 °C. The conversion gives a maximum yield of 88% when transesterification is allowed to continue for 120 min. The waste cooking oil used in this work is dominated with linoleic acid and oleic acid, which during transesterification gets converted into methyl linoleate and 9-octadecenoic acid methyl ester. These nanocatalysts are fabricated using a composite of rutile (tetragonal) phase SnO_2 and cubic phase MgO nanostructures with prominent crystal orientation along [211] and [200] plane respectively. The MgO-SnO_2 nanocomposites with an enhanced surface area of 31 m^2/g, basic sites of 2 mmol/g, and particle size of ~15 nm are synthesized by novel sequential thermal decomposition and sol-gel technique. The synthesized wide band gap nanocomposites have Mg and Sn in the ratio of 15:1 and do not have any impurity phases as observed in the X-ray diffraction pattern and EDS spectrum. The presence of surface oxygen states and Mg^{2+} and Sn^{4+} oxidative states is responsible for the catalytic activity and recyclability displayed by the composites. This work signifies the role of nanocomposites and their synthesis conditions in improving the rate of transesterification. These metal oxide nanocomposites which are nontoxic, stable, cost effective, and easier to synthesis are promising catalysts for large-scale transesterification of waste cooking oil to biodiesel.

Keywords: MgO-SnO_2 nanocomposite, Transesterification, Biodiesel, Waste cooking oil

Introduction

The demand for fuel in transportation sector is growing due to the industrialization and population. The increasing demand fueled by shortage of depleting energy sources (fossil fuels) [1] has forced us to find alternative renewable source of energy such as biodiesel [2] which is made of mono-alkyl esters of long-chain fatty acids derived from vegetable oils and animal fats. Biodiesel is obtained by transesterification of vegetable oil or animal fat with alcohol (preferably methanol) in the presence of a catalyst. The stoichiometry of the transesterification reaction needs 3 mol of

alcohol and 1 mol of triglyceride to give 3 mol of fatty acid methyl esters and 1 mol of glycerin which is given by Eq. 1 in which R_1, R_2, and R_3 are known as the fatty acid chains made of long-chain hydrocarbons [3].

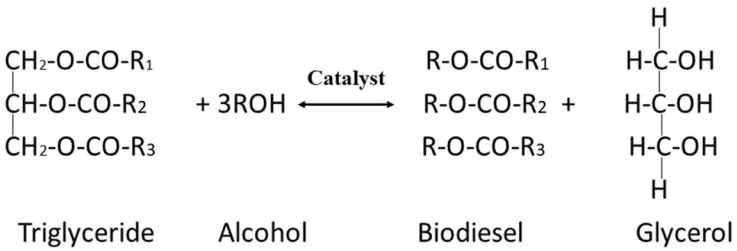

(1)

Biodiesel with its high biodegradability, flash point, cetane number, calorific value, lubricity, low emission of particulate matter, and greenhouse gases is best suited as an alternative fuel [4]. However, reducing their production cost is challenging due to the high cost of feedstock. Hence, waste cooking oil (WCO) can be used to replace other expensive feedstock to produce biodiesel. WCO collected from various sources such as restaurant, canteens, and rendered animal fats are cheaper than edible oils.

WCO generated by each country is large, and it is not safe for human consumption. Since the year 2002, European Union has banned the reuse of cooking oil as an additive to the feeding mixture for animals since the compounds which are formed during heating of the oil are harmful, and it will enter the food chain in the form of animal meat [5]. Disposal of WCO is difficult as it contaminates the groundwater and blocks the sewage pipelines. Hence, the conversion of WCO into biodiesel serves as a promising source of clean energy and method for reducing environmental pollution due to oil disposal issues.

Transesterification reaction is a tedious process as it involves two immiscible phases, oil and methanol, and the efficiency of conversion of WCO to biodiesel depends on the type of catalyst. Both homogenous and heterogeneous catalysts can be used in the transesterification process.

However, heterogeneous catalysts are more advantageous when compared to the homogenous catalyst since the recovery and reusability of the catalyst for both batch and continuous process are easier. Heterogenous catalyst are eco-friendly and noncorrosive and can be easily separated from the product. Heterogenous catalyst requires lesser number of steps in product purification since it does not produce soap. It does not create much disposal problems when compared to homogenous catalyst. Heterogenous catalyst having both acid and basic site can serve as a bifunctional catalyst which can carry out esterification and transesterification simultaneously. Emil Akbar et al. have obtained 99% efficiency of biodiesel while converting Jatropha oil using Na-doped SiO_2 solid catalyst at reflux temperature of methanol 65°C, 1:15 molar ratio of methanol to oil, and 6 wt% of catalyst. Na-doped SiO_2 solid catalyst played the role of alternative to homogenous catalyst and showed enhanced catalytic activity under mild conditions in a shorter duration of time (45 min) [6]. Chakraborty R. et al. have reported that biodiesel yield of 97.73% was obtained from sunflower oil using inexpensive heterogenous catalyst calcined fish (*Labeo rohita*) scale. The calcined fish

(*L. rohita*) scale catalyst possesses high surface area and basicity under high reaction time, and enhanced yield of biodiesel was attained at low catalyst concentration and methanol to oil molar ratio [7].

Metal oxide nanoparticles which are easier to synthesis are being widely used as catalysts due to its improved catalytic efficiency, reusability, and high surface area [8]. Metal oxide heterogenous catalyst is made up of positive metal ions which perform the role of electron acceptors and negative oxygen ions which perform as proton acceptors. This enhances the transesterification reaction and gives adsorptive sites for methanol in which the O–H bonds breaks down into methoxide anions and hydrogen cations. The methoxide anion present in the heterogenous catalyst further reacts with the triglyceride molecules to give fatty acid methyl esters [9]. The basic heterogenous catalysts are successful when compared to other heterogeneous materials due to the formation of methoxide ions, but it is affected by leaching during the transesterification reaction.

Nanocomposites solve this problem since a stable metal oxide is added to the active metal oxide, hence finds various industrial applications [10] in food, biomedical, engineering, electroanalysis, energy storage, wastewater treatment, catalysis, automotive, etc. [11]. Nanocomposites are well suited for transesterification reaction due to its high specific surface area, catalytic activity, and selectivity [12]. Furthermore, they help in improving the product quality and require less reaction temperature and time. The surface acidity of the nanocomposite makes it a good solid catalyst with enhanced catalytic activity that sustains for a longer duration [13].

Metal oxide nanocomposites are cheaper and efficient as catalyst. It has been reported that sulfonated tin oxide when used as catalyst in the transesterification of palm fatty acid distillate gives a biodiesel yield of 93.8% under optimum conditions of 9:1 methanol to palm fatty acid distillate molar ratio, 4 wt% of catalyst amount, and 100 °C reaction temperature in a duration of 3 h [14]. Similarly, pure tin oxide (SnO_2), which has both Lewis-acidic and basic sites, in which Sn ions contribute to the Lewis acid sites and surface hydroxy groups or oxide ions contribute to the basic sites [15], also shows good catalytic performance in transesterification as well as esterification reactions.

It has been reported that biodiesel yield of 82.8% is obtained from *Ulva lactuca* seaweeds using TiO_2-ZnO nanocomposite catalysts under optimum conditions of 4 wt% catalysts at reaction temperature of 60 °C in a duration of 4 h [16]. Abdelrahman has reported that diatomite supported by CaO-MgO composite when used as a catalyst in transesterification reaction gives a yield of 96.47% under optimum conditions of 1:15 oil to methanol ratio, 6 wt% of catalyst at 90 °C in a duration of 120 min. Diatomite shows extraordinary physical properties such as low bulk density, increased porosity, high surface area, greater insulation, and relative inertness. These properties increase the economic and industrial value of make diatomite deposits [17].

Mufsir et al. have reported that ZnCuO/(30%) NDG catalyst gives 97.1% yield of biodiesel from waste cooking oil at the optimized conditions of 10 wt% catalyst loading, 15:1 methanol:oil molar ratio, 8 h reaction time, and 180 °C reaction temperature [18]. Integration of n-doped graphene in the nanocomposite enhances the catalytic activity of mixed metal oxides since graphene-based materials possess high surface area, porosity, and electrical conductivity. Adeyinka et al. have reported that biodiesel yield of 83.16% was attained from waste cooking oil at the optimized conditions of 66.54 °C reaction

temperature, 17.99:1 methanol to oil ratio, 2 h reaction time, and 0.5 wt% of catalyst loading using zinc-modified anthill composite [19].

Borah et al. have reported that TiO_2-RGO nanocomposite when used as a heterogenous catalyst in the transesterification of WCO gives a yield of 98% under optimum conditions of 1:12 oil to methanol molar ratio, 1.5 wt% catalyst loading at a reaction temperature of 65 °C for a reaction duration of 3 h. This improved catalytic activity is due to the enhanced surface area [20]. WSA/ZnO/K_2CO_3 composite is used as a catalyst in the transesterification of *Moringa* oleifera nonedible oil which gives a yield of 97.34% under optimum conditions of reaction temperature of 65 °C, a reaction time of 4 h, a catalyst content of 4 wt%, and methanol to oil ratio of 18:1 [21].

Nisha Bayal et al. have reported on the synthesis of SnO_2-MgO nanoparticles by sol-gel method and measured the photocatalytic activity towards methylene blue degradation. SnO_2-MgO nanoparticles exhibits an average particle size of ~9.8 to 13.4 nm, and bandgap was found to vary between 3.43 and 3.98 eV. The author has reported that crystallite size of SnO_2 decreases on increasing the content of magnesium. Excess amount of MgO in mixed metal oxide nanoparticles covers the surface of SnO_2, hence reduces the photocatalytic degradation of the dye [22]. Hina et al. have reported that MgO-SnO_2 can be synthesized by hydrothermal method and used as a catalyst to degrade 2,4-dinitrophenylhydrazine (DNPH) [23].

There is no open literature on the usage of MgO-SnO_2 as nanocatalyst for the transesterification reaction. In the present work, we grow SnO_2 nanoparticles on MgO nanoparticles to form MgO-SnO_2 nanocomposite by sol-gel method for transesterification of WCO to biodiesel. Due to low surface area of MgO, it is not used in pure form as a catalyst [24]. Hence, it is combined with SnO_2 to obtain MgO-SnO_2 nanocomposite with enhanced surface area. Moreover, the presence of MgO along with SnO_2 helps to stop the recombination of holes and electrons [22]. Hence, free electrons are available for the reaction. MgO-SnO_2 nanocomposite has been reported to possess increased basic sites on the surface due to the defects in MgO and the presence of SnO_2 [25]. Furthermore, by embedding SnO_2 with MgO nanoparticles, the agglomeration of SnO_2 particles can also be prevented. MgO-SnO_2 catalyst is active for transesterification since SnO_2 has both Lewis-acidic and basic sites and MgO has high basicity. X-ray diffraction (XRD), Fourier-transform infrared spectroscopy (FT-IR), UV-vis spectroscopy, Brunauer–Emmett–Teller (BET) studies, high-resolution transmission electron microscopy (HR-TEM), energy-dispersive X-ray spectroscopy (EDS), X-ray photoelectron spectroscopy (XPS), and gas chromatography-mass spectrometry (GC-MS) were employed for the characterization of synthesized catalyst and converted biodiesel. The kinetic studies of the reaction were carried out to find out the order of the reaction.

Methods

Materials and catalyst preparation

Chemicals needed for the synthesis of nanocatalyst are magnesium acetate tetrahydrate ($Mg(CH_3COO)_2{\cdot}4H_2O$), absolute ethanol ($C_2H_5OH$), oxalic acid dihydrate ($C_2H_2O_4{\cdot}2H_2O$), tin (II) chloride dihydrate ($SnCl_2.2H_2O$), and absolute methanol (CH_3OH) which are purchased from Sigma–Aldrich with purity > 99.9%. The transesterification reaction was performed using WCO collected from canteen kitchen.

Synthesis of magnesium oxide nanocatalyst by sol-gel method

The methodology for synthesis of MgO is reported elsewhere [26]. Magnesium acetate tetrahydrate (1.65 M) of mass 53.2075 g was dissolved in 150 ml of absolute ethanol under constant stirring in a magnetic stirrer for 2 h. The stirring was continued until the particles were completely dissolved and form a milky white solution. A total of 1 M oxalic acid dihydrate was added dropwise into the milky white solution until the pH drops to 5. This mixture was continuously stirred for few hours until it thickens into a white gel. The obtained gel was left overnight for further gelation and dried in an oven at 100 °C for 15 h. The dried sample was ground using mortar and pestle to produce a fine powder. Calcinating this powder at high temperature (600 °C, 2 h) results in the formation of MgO nanostructures.

Synthesis of tin oxide nanoparticles by thermal decomposition method

A total of 1.15 g of tin (II) chloride dihydrate was weighed in a silica crucible and then heated in a muffle furnace at decomposition temperature of 600 °C for a reaction time of 20 min, and gray color fine powder is obtained upon completion of the reaction.

Synthesis of MgO-SnO_2 nanocomposites

SnO_2 nanoparticles were synthesized by thermal decomposition of tin (II) chloride dihydrate (4 g) at 600 °C for 20 min. Magnesium acetate tetrahydrate (53.2075 g) was initially dissolved in 100 ml of ethanol under constant stirring using a magnetic stirrer. The ratio of MgO to SnO_2 was kept at 15:1; SnO_2 (0.4 g) synthesized by thermal decomposition is dispersed in 50 ml of absolute ethanol. The SnO_2 solution was added dropwise to the earlier mixture of magnesium acetate and ethanol. The pH of the solution was adjusted to 5 using 1 M oxalic acid dihydrate ($C_2H_4O_2.2H_2O$). The mixture was continuously stirred until a thick gel was formed. The gel formed was left overnight for further gelation process before being dried in an oven at 100 °C for 15 h. The dried materials were ground using mortar and pestle to produce fine powder. Subsequently, these particles were calcinated at 600 °C for 2 h to form MgO-SnO_2 nanocomposites.

Characterization of MgO-SnO_2 nanocomposites

The powder X-ray diffraction (XRD) spectrum for the synthesized samples was documented on a PANalytical X'Pert Pro diffractometer using Cu–Kα radiation (λ = 0.154065 nm). JCPDS (Joint Committee of the Powder Diffraction Standard) database files were used to identify the phases present in the sample. The nanocomposite structure formation was studied using high-resolution transmission electron microscopy (HRTEM) images (FEI Company of the USA, model: Tecnai G2 F30 S-Twin (FEG-based TEM)). The particle size was measured using the quantitative tools in the ImageJ software. Elemental composition and phase of these nanoparticles were confirmed using energy-dispersive spectroscopy (EDS). Optical absorption studies were performed using UV-vis spectrophotometer (Agilent, Cary 60), and band gap energy of the nanocomposites was recorded. Fourier-transform infrared spectroscopy (FTIR) was studied for the nanocomposites in the region of 400–4000 cm^{-1}

using a FTIR spectrometer (Thermo Nicolet, model number: 6700) with KBR pellet method. Brunauer–Emmett–Teller (BET) surface area analysis was carried out using Micromeritics ASAP 2020 with degassing conditions of 150 °C and 100 mm Hg for 180 min and degassing ramp rate of 10 °C/min and 50 mmHg/s with a vacuum set point of 500 μm Hg with evacuation time of 60 min. The surface composition of the synthesized nanocomposite was analyzed using X-ray photoelectron spectroscopy (K-Alpha-KAN9954133, Thermo Scientific).

Transesterification of waste cooking oil

The transesterification of WCO was carried out in a closed beaker in a hot plate setup with a magnetic stirrer. Basic sites of MgO-SnO_2 were found out to be 2 mmol/g using back titration method [27, 28]. Required amount of MgO-SnO_2 nanocatalyst was added to the beaker and then stirred along with methanol for a duration of 30 min. The desired quantity of pretreated WCO was added to the beaker, and transesterification was carried out at required reaction temperature along with the premixed solution consisting of methanol and nanocatalyst. The reaction mixture was filtered using a Whatman filter paper and centrifuged to separate the catalyst at the end of the reaction. The mixture was poured into a separating funnel and allowed to stand for 24 h to separate the biodiesel in the upper layer and glycerol in the bottom layer. Obtained biodiesel was heated at 80 °C in a vacuum oven for 24 h to remove the moisture and unreacted methanol. Transesterification reaction conditions were optimized by changing the parameters such as methanol to oil molar ratio (9:1 to 21:1), catalyst concentration (1–4 wt%), reaction duration (30–180 min), and reaction temperature (40–80 °C), respectively. Gas chromatography-mass spectroscopy (GC-MS) was used to detect the conversion of biodiesel and the presence of monoglycerides, diglycerides, and unreacted triglycerides. The yield of biodiesel from the waste cooking oil was found out using the Eq. 2 given by the following:

$$\text{Yield of biodiesel} = \left(\text{weight of fatty acid methyl esters/weight of oil}\right) \times 100 \quad (2)$$

Characterization of waste cooking oil and biodiesel

WCO was filtered with a fine cloth to remove all the insoluble impurities and then heated at 110 °C to remove the moisture. The pretreated WCO was stored in an airtight container for further use. The acid value, density, and average molecular weight of the waste cooking oil were found out to be 3.52 mg KOH g^{-1}, 0.92 g/ml, and 870 g/mol. Fourier-transform infrared spectroscopy (FT-IR) and gas chromatography along with mass spectrometry (GC-MS) were used to confirm the conversion of waste cooking oil into biodiesel. Gas chromatography-mass spectrometry was carried out in Agilent 7890a gas chromatograph equipped with a 30 m HP-5 MS column of internal diameter 0.25 mm and 0.15 μm film thickness. Sample was introduced in split injection with a split ratio of 50:1. The oven temperature was started at 25 °C and then ramped at 50 °C per min to 230 °C withhold time of 3 and 5 min, respectively. Helium gas was introduced at the rate of 1 μl/min in a constant mode. The fatty acid composition of the waste cooking oil obtained from GC-MS spectra is palmitic acid (9.47%) and stearic acid (6.76%) which are considered to be saturated fatty acid, linoleic acid (56.27%) which is a polyunsaturated fatty acid, and oleic acid (27.51%) which is a monounsaturated fatty acid. GC-MS spectra

of biodiesel show the presence of fatty acid methyl ester peaks which is identified and confirmed with the help of NIST library 11.

Results and discussion

Structural and optical properties of MgO-SnO_2 nanocomposites

MgO-SnO_2 nanocomposites were synthesized by sol-gel method. Figure 1 shows the X-ray diffraction pattern of MgO-SnO_2 nanocomposites, with crystal plane orientations of both MgO and SnO_2 nanoparticles, but do not show the formation of any composite phases. The SnO_2 in nanocomposite has orientation along the [110], [101], [301], and [321] planes corresponding to the rutile (tetragonal) phase, and MgO particles have orientation along [111], [200], [311], and [222] planes corresponding to the cubic. The peak corresponding to [222] plane orientation of MgO [29] and [321] plane of SnO_2 overlaps each other leading to peak broadening. As calculated using Scherrer formula, the crystallite size of MgO and SnO_2 nanoparticles present in the nanocomposite is ~12 nm and ~8 nm, respectively, which is the same as that of pure nanoparticles.

Figure 2a shows the HRTEM image of the MgO-SnO_2 nanocomposites, showing the distinct presence of MgO and SnO_2. The particle size estimated from the HRTEM image is ~15 nm for MgO and ~13 nm for SnO_2 nanoparticles. Figure 2b shows the diffraction pattern obtained from HRTEM indicating high-order crystallinity with the d-spacing corresponding to the orientation along [211] and [311] planes of both MgO (cubic) and SnO_2 (tetragonal) nanoparticles respectively.

Figure 3 shows the Tauc plot of MgO-SnO_2 nanocomposite structures. The calculated bandgap for MgO-SnO_2 nanocomposites shows two linear fit regions indicating bandgaps at ~3 eV and 5.2 eV corresponding to MgO and SnO_2 nanoparticles. The

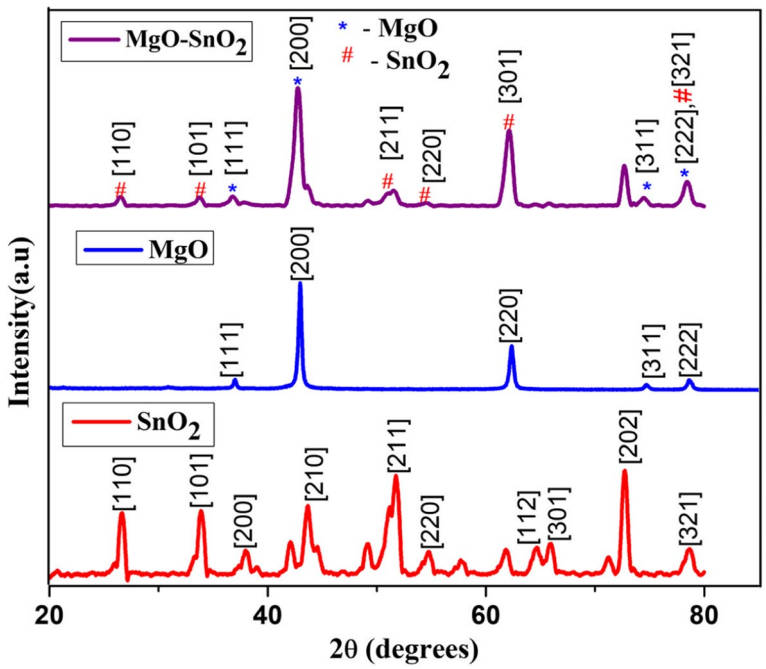

Fig. 1 X-ray diffraction pattern of MgO-SnO_2 nanocomposites under thermal decomposition (600 °C) for 20 min and calcination at 600 °C for 2 h

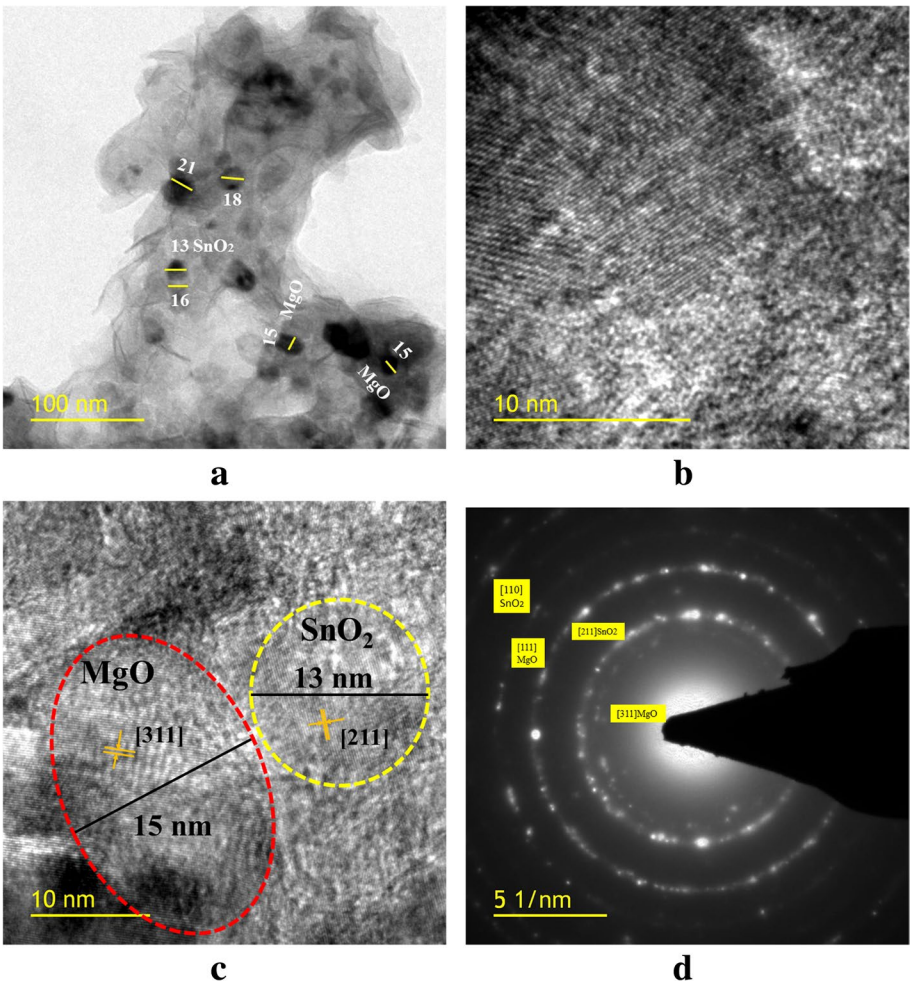

Fig. 2 **a**, **b**, and **c** HR TEM image of MgO-SnO_2 nanocomposite showing particles of size ~15 nm **d** SAED pattern showing planes of MgO ([311], [111]) and SnO_2 ([110], [211])

bandgap of MgO nanoparticles, both in pure and hybrid form, is the same; however, there is a blue shift in the bandgap of SnO_2 nanoparticles in the hybrid structure (~5.2 eV) when compared to that of pure SnO_2 nanoparticles (~3.5 eV).

Figure 4 shows the FTIR spectrum of MgO-SnO_2 nanocomposites with absorption peak at ~480 cm^{-1} which is due to the overlap of vibrational modes at ~450 cm^{-1} (MgO) [30], ~491 cm^{-1}, and 626 cm^{-1} (SnO_2) [31]. The vibrational modes of O–H bond at 1419 cm^{-1}, 1635 cm^{-1}, and 3432 cm^{-1} [32, 33], which were present in pure MgO nanoparticles, have been quenched in the nanocomposites. The quenching of O–H bonds occurs when the MgO precursors are calcinated at 600 °C along with SnO_2 nanoparticles. These SnO_2 particles undergo repeated thermal decomposition by utilizing the OH content in magnesium acetate solution.

EDS analysis of the samples shows the elemental composition and phase purity of MgO-SnO_2 samples. From EDS analysis shown in Fig. 5, it is inferred that the

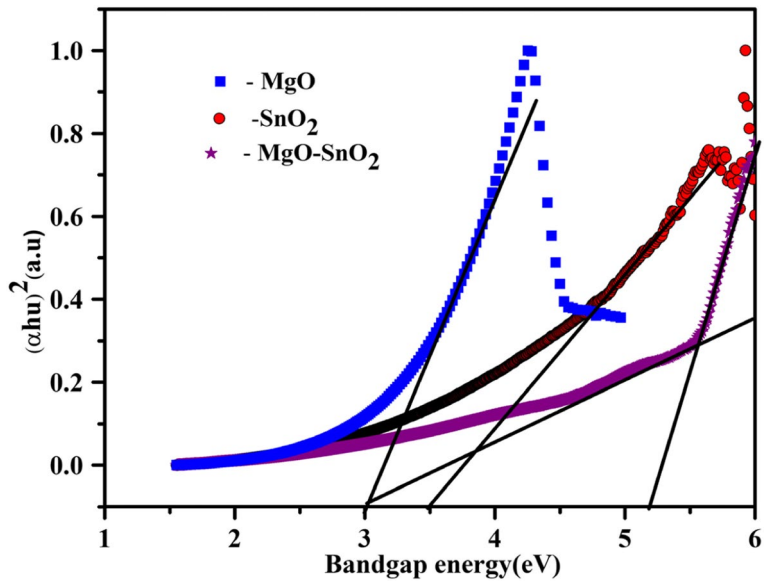

Fig. 3 Comparison of UV-visible absorption spectra of MgO, SnO_2, and MgO-SnO_2 with calcination 600 °C for 2 h and thermal decomposition at 600 °C for 20 min

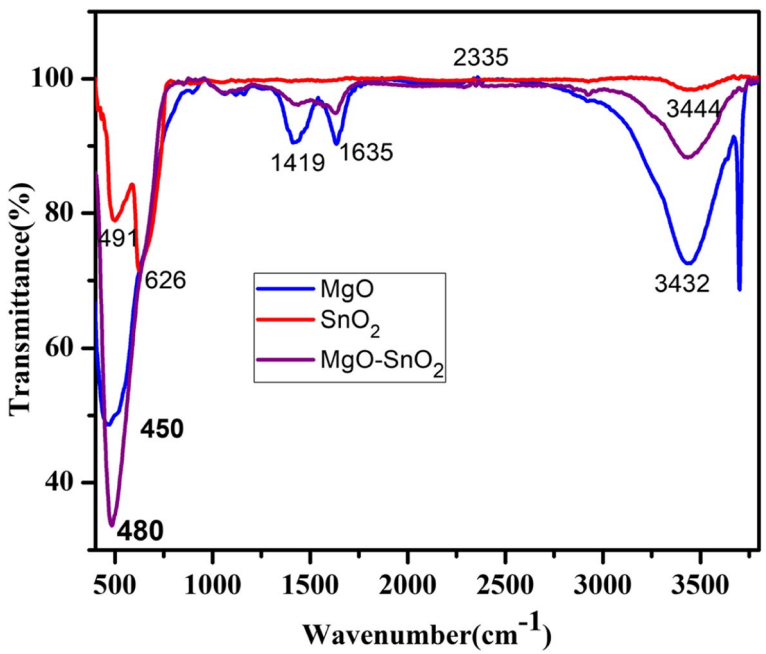

Fig. 4 Comparison of FTIR spectra of MgO, SnO_2, and MgO-SnO_2

elements of this nanocomposite are magnesium, tin, and oxygen with Mg to Sn ratio 15:1 which is the same as the ratio taken during the synthesis of the hybrids. The hybrid sample contains 65.38% of Mg and 7.69% of Sn in the structure (Table 1).

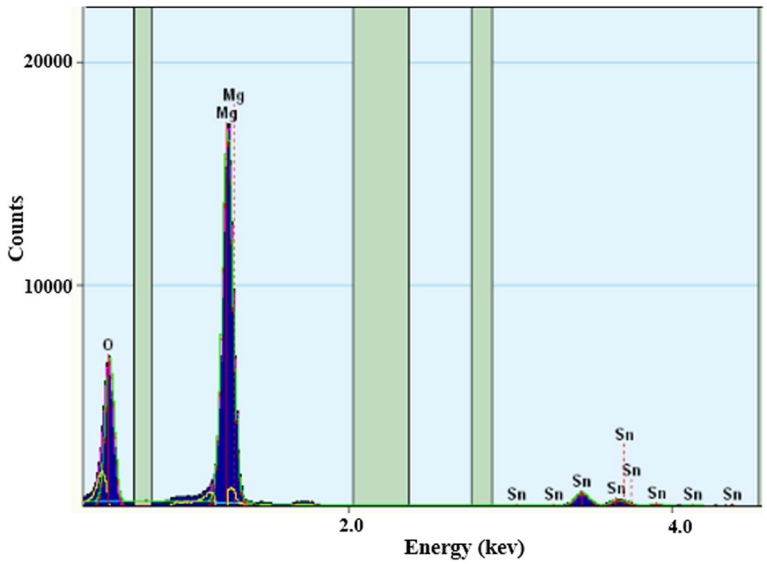

Fig. 5 EDS map for MgO-SnO_2 nanocomposite

Table 1 Elemental analysis of MgO-SnO_2 nanocomposite

S. no	Elements	Weight percentage (%)	Atomic percentage (%)
1	Mg	65.38	60.92
2	Sn	7.69	1.44
3	O	26.92	37.62

BET analysis

BET analysis was carried out for finding out the surface area (nm/g), pore size (nm), and pore volume (mL/g) of MgO-SnO_2 nanocomposite. The analysis was performed at 150 °C and 100 mmHg for a duration of 180 min and degassing ramp rate of 10 °C/min and 50 mmHg/s with a vacuum set point of 500 μHg with evacuation time of 60 min. The nitrogen physisorption isotherms were observed at liquid nitrogen temperature between P/P_o of 0.05 to 0.989. The size of the nanocomposite can be found out theoretically using Eq. 3 assuming particles are spherical.

$$D_{BET=\frac{6000}{\rho S}} \tag{3}$$

where S denotes the surface area in m^2/g, ρ is the density of the nanomaterial in g/cm^3, and D_{BET} is the equivalent particle diameter in nanometers.

The surface area, pore size, and pore volume of MgO nanoparticles were 16.3 m^2/g, 16.5 nm, and 0.05 ml/g, whereas MgO-SnO_2 nanocomposite shows an enhancement in surface area (31.6 m^2/g), pore size (23.9 nm), and pore volume (0.19 ml/g). Increased pore size and pore volume reduce the diffusion of molecules with long alkyl chain when MgO-SnO_2 nanocomposites take part as catalyst in transesterification process. For catalytic reaction, mesoporous particles with pore size in the range of 10–50 nm are highly preferred. Hence, MgO-SnO_2 nanocomposite is more suitable for catalytic reactions.

Similar works on the biodiesel production using diatomite@CaO/MgO catalyst which possess higher surface area of 134.85 m^2/g than raw diatomite nanocomposite (117 m^2/g) have been reported. The enhanced surface area of the nanocomposite gives biodiesel yield of 96.47% after 120 min at 90 °C using 6 wt% catalyst and 15:1methanol to oil ratio [17].

X-ray photon spectroscopy is used for finding out the surface composite elements, purity, and chemical state of the synthesized sample. The peaks which are found on the survey spectrum in Fig. 6a of MgO-SnO_2 nanocomposite show mainly Mg, Sn, and O except for C element which confirms the high purity of MgO-SnO_2 nanocomposite. Figure 6b shows Mg 1 s peak deconvoluted at 1303.23 eV, 1304.26 eV is assigned to MgO [34] with Mg^{2+} valence state in MgO-SnO_2 nanocomposite, and it is found to be matching with the literature value for MgO nanoparticles [35, 36], and 1306.69 peak corresponds to the Mg-OH [37]. O 1 s peak for MgO-SnO_2 nanocomposite can be deconvoluted into two peaks as shown in Fig. 6c. The lower binding energy peak at 531.04 eV is due to the lattice oxygen of MgO-SnO_2 nanocomposite, whereas the higher binding energy peak at 534.27 eV is due to absorbed oxygen ions on the surface [38–40]. Figure 6d shows Sn 3d spectrum from which the peaks for Sn are seen at 486.63 eV and 494.91 eV which is due to Sn $3d_{5/2}$ and $3d_{3/2}$ corresponding to the standard data for SnO_2, and the satellite peaks at 489.17 eV and 497.47 eV correspond to Sn $3d_{5/2}$ and Sn $3d_{3/2}$.

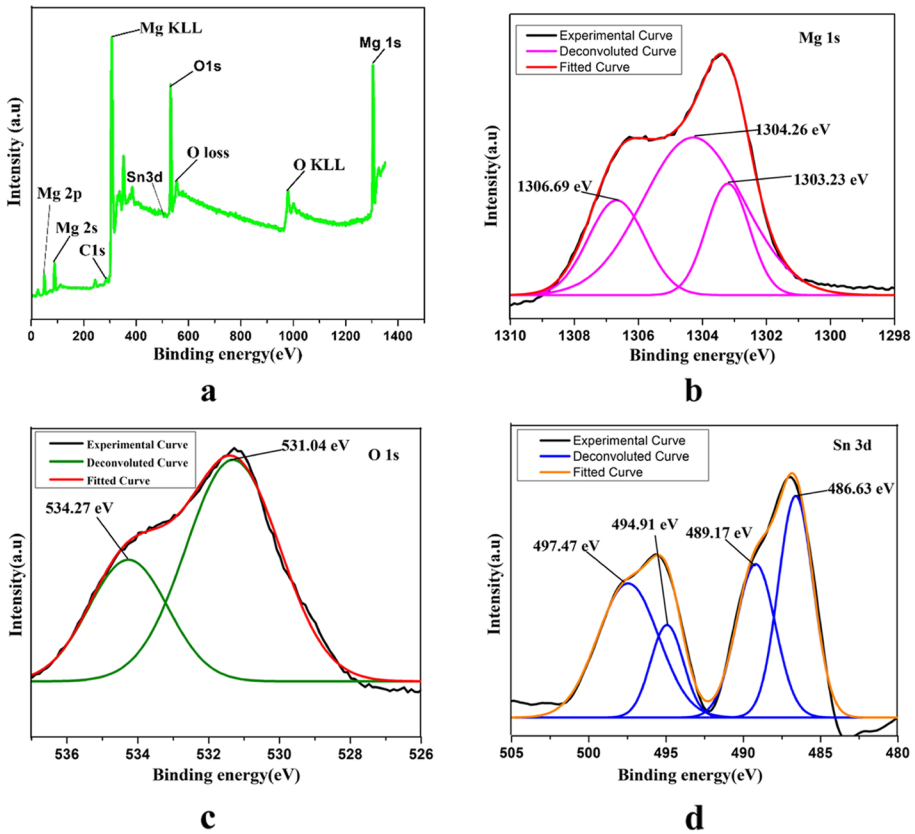

Fig. 6 **a** XPS spectrum of MgO-SnO_2 nanocomposite and XPS spectra of **b** Mg 1s core level, **c** O 1s core level, and **d** Sn 3d core level for MgO-SnO_2 nanocomposite

The spin-orbit splitting of 8.28 eV shows the presence of Sn^{4+} in SnO_2. The presence of Sn^{+2} or Sn^{+0} is not seen in the spectrum. The synthesis of MgO-SnO_2 nanocomposites is carried out at relatively low temperature (600 °C). Hence, the formed nanoparticles retain their individual characteristics and do not form compounds.

Optimization of various parameters for biodiesel production using MgO-SnO_2 nanocomposite

Effect of amount of catalyst loading on biodiesel yield using MgO-SnO_2 nanocomposite

Amount of nanocatalyst added during the transesterification reaction plays an important role that decides the yield of biodiesel. Hence, the amount of the nanocatalyst was optimized to enhance the yield of biodiesel keeping the reaction temperature at 60 °C, methanol to oil ratio at 18:1, and reaction duration of 2 h. Nanocatalyst when used in the transesterification reaction alters the rate of the reaction, but it does not change the equilibrium conversion for a reversible reaction [41]. Figure 7 shows the effect of MgO-SnO_2 nanocomposite loading on the yield of biodiesel at the noted reaction conditions. MgO-SnO_2 nanocomposite loading was changed in the range of 0–4 wt%. Transesterification results show that on increasing the amount of catalyst from 1 to 2 wt%, biodiesel yield also increases from 85 to 88% which suggests that the transesterification reaction is dependent on the amount of catalyst. Enhanced biodiesel yield of 88% is obtained at 2 wt% of nanocatalyst loading. Biodiesel yield starts to decrease to 82% and 78% as the amount of catalyst loading is changed from 3 to 4 wt%. At higher amount of catalyst loading, the converted biodiesel gets adsorbed on the catalyst surface which in turn decreases the yield of the biodiesel, and moreover, the solution will become more viscous which creates problem while mixing the reactants and the solid catalyst [42]. On increasing the amount of catalyst, there is a decrease in biodiesel yield which is due to aggregation of the catalyst which in turn decreases the contact between the active sites

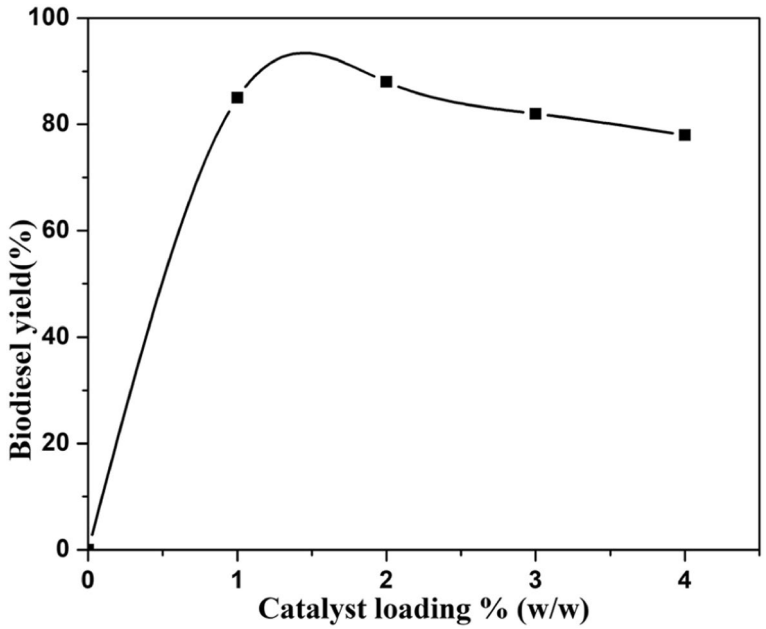

Fig. 7 Effect of catalyst amount (wt%) on biodiesel yield (%)

and reactants. Higher catalyst loading also decreases the biodiesel yield because it causes soap formation which is due to the dissolution of ester in glycerol. Moreover, higher catalyst loading decreases the biodiesel yield because it makes the product stickier which hinders the mass transfer in liquid (waste cooking oil) — liquid (methanol) — solid (catalyst) structure. Hence, 2 wt% of MgO-SnO_2 nanocomposite with the biodiesel yield of 88% was chosen for further transesterification of WCO into biodiesel.

Effect of methanol to oil ratio on biodiesel yield using MgO-SnO_2 nanocomposite

The molar ratio of methanol to oil is one of the parameters that affects the conversion of WCO into fatty acid methyl esters. Molar ratio of methanol to triglyceride needed for transesterification reaction stoichiometrically is 3:1, whereas higher molar ratio will increase the biodiesel yield since it shifts the equilibrium towards the biodiesel formation. The effect of methanol to oil molar ratio was studied from 9:1 to 21:1. At lower methanol to oil ratio (< 9:1), the transesterification reaction was incomplete and does not result in biodiesel conversion. Figure 8 shows the effect of methanol to oil molar ratio on the biodiesel yield. It can be inferred (Fig. 8) that yield of biodiesel increases with increase in methanol to oil molar ratio which is due to the increase in contact between the methanol and oil molecules [43]. Maximum biodiesel yield of 88% is obtained for 18:1 methanol to oil ratio at a reaction temperature of 60 °C for a duration of 2 h with 2 wt% of nanocatalyst. On further increase in methanol to oil molar ratio to 21:1, there is a drop in biodiesel yield to 85% which is due to the dilution in the concentration of oil [44, 45]. Moreover, excess amount of methanol increases the dissolution of glycerol and creates difficulty, while separation of the product from the glycerine after the transesterification also needs longer duration of time for separation of the product [46]. When glycerine is present in the solution, it hinders the reaction of methanol with the reactants (waste cooking oil and catalyst) and promotes reversible reaction which in turn decreases the biodiesel yield. Increased methanol to oil ratio affects the biodiesel quality

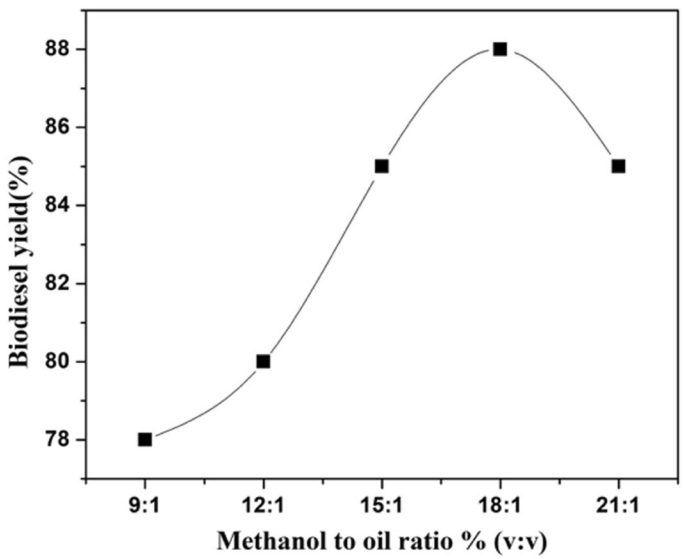

Fig. 8 Effect of methanol to oil molar ratio % (v:v) on biodiesel yield (%)

by decreasing its viscosity, flash point, and density due to the presence of methanol along with the fuel [47]. Abdullah et al. have reported that biodiesel with very low viscosity will not be able to give sufficient lubrication on the oil injection pump, which further results in leakage in the fuel injection pump [48].

Effect of reaction temperature on biodiesel yield using MgO-SnO_2 nanocomposite

The reaction temperature plays an important role in reducing the cost of production. Figure 9 shows the effect of reaction temperature (40 to 80 °C) on biodiesel yield keeping methanol to oil ratio at 18:1, 2 wt% of nanocatalyst carried out for a reaction duration of 2 h. The yield of biodiesel shows an increase with increase in temperature and reaches a maximum yield of 88% at 60 °C. This is due to the accelerated chemical reaction that enhances the collision among the reactant molecules, thereby increasing the miscibility and mass transfer [49]. Biodiesel yield starts to decrease from temperature of 70 °C onwards. The reduction in the yield of biodiesel at higher temperature is due to the increased miscibility between the product and glycerine which decreases the phase separation and hence yield. Moreover, at higher temperatures, vaporization of methanol is high, since boiling point of methanol is 65 °C, and hence, it is present in vapor phase, and polarity of methanol reduces which further reduces the amount of methoxide species in the transesterification reaction [50]. While at the reaction temperature lower than 40 °C, the activation energy is not sufficient to encourage collisions between the reactant molecules, whereas at higher temperature (> 65 °C), there is an increase in the particle kinetic energy due to the absorption of heat, and many of the reactant molecules possess the minimum energy to collide and react; hence, the activation energy is attained easily.

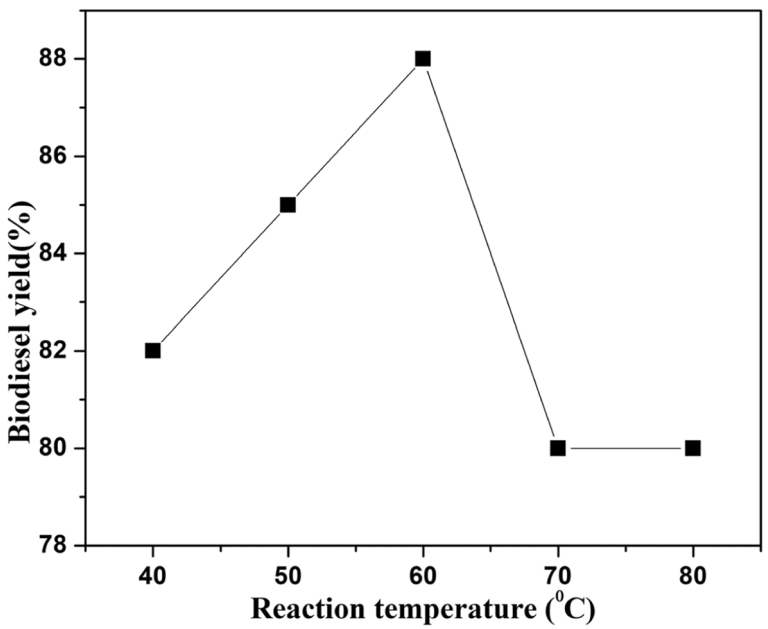

Fig. 9 Effect of reaction temperature (°C) on biodiesel yield in %

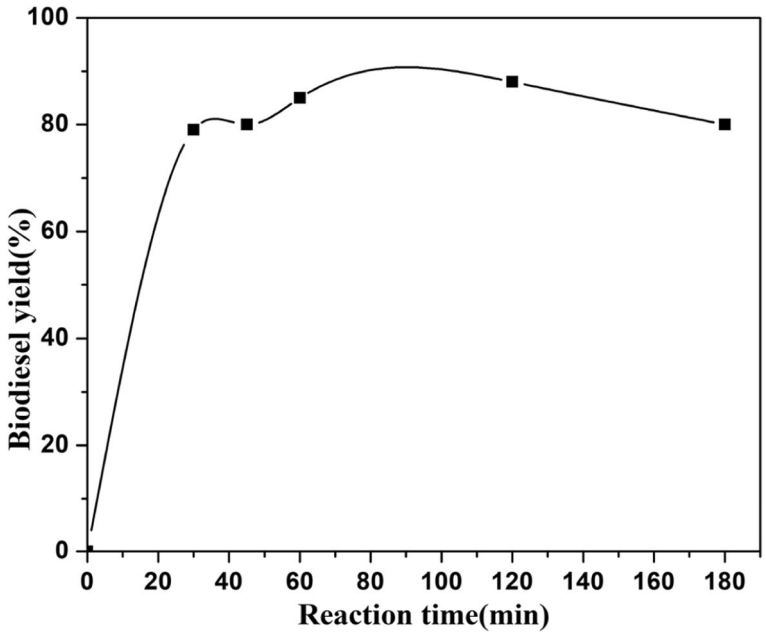

Fig. 10 Effect of reaction duration (min) on biodiesel yield in %

Effect of reaction time on biodiesel production using MgO-SnO_2 nanocomposite

Reaction time plays an important role in the transesterification reaction of WCO into biodiesel using MgO-SnO_2 nanocomposites. Figure 10 shows the effect of reaction time on biodiesel yield which is carried out at optimum conditions of methanol to oil ratio (18:1), 0.1 g of nanocatalyst, and at reaction temperature of 60 °C. It was concluded from the experiment that the biodiesel yield increases from 79 to 88% for a duration of 0 min to 2 h. This increase in biodiesel yield is due to the forward reaction, or production of biodiesel is very rapid until the equilibrium is attained [51]. Further increase in duration results in prolonged exposure of the catalyst and methanol leading to decrease in the yield of the biodiesel due to the backward reaction which affects the separation of the formed esters and hence the yield of the biodiesel decreases [44].

Reusability of the catalyst on biodiesel production using MgO-SnO_2 nanocomposite

The stability and reusability of the catalyst are the important parameters which reduce the biodiesel production cost. The reusability of the catalyst is carried out at optimum conditions of methanol to oil ratio (18:1), 0.1 g of nanocatalyst, and reaction temperature of 60 °C for a duration of 2 h and is shown in Fig. 11. The reaction mixture was centrifuged to separate the catalyst at the end of the transesterification. Acetone is added to the recovered catalyst which is further sonicated and then centrifuged. This procedure is followed for 4 times until the unreacted waste cooking oil and glycerol are removed from the catalyst surface. The sample is allowed to dry in room temperature. The used catalyst is not calcinated or heated before the next cycle since the structural properties of the catalyst will undergo change during calcination. Biodiesel yield does not change significantly up to second cycle of usage. Later, it starts to decrease from 87 to 84% at fourth cycle of usage. This may be due to the change in basic sites, structure, and surface area of the nanocatalyst or due to coating of organic matter layers on the surface of the

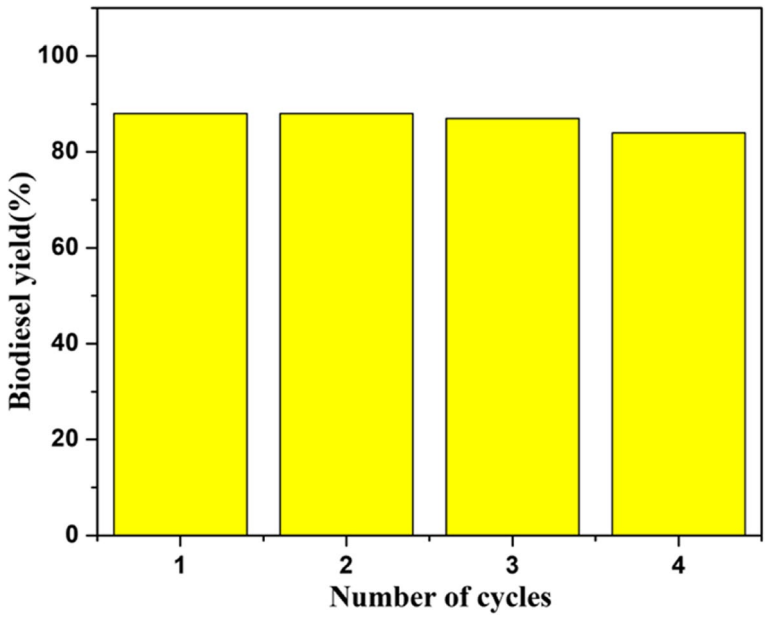

Fig. 11 Reusability of MgO-SnO_2 nanocomposite carried out at optimum conditions

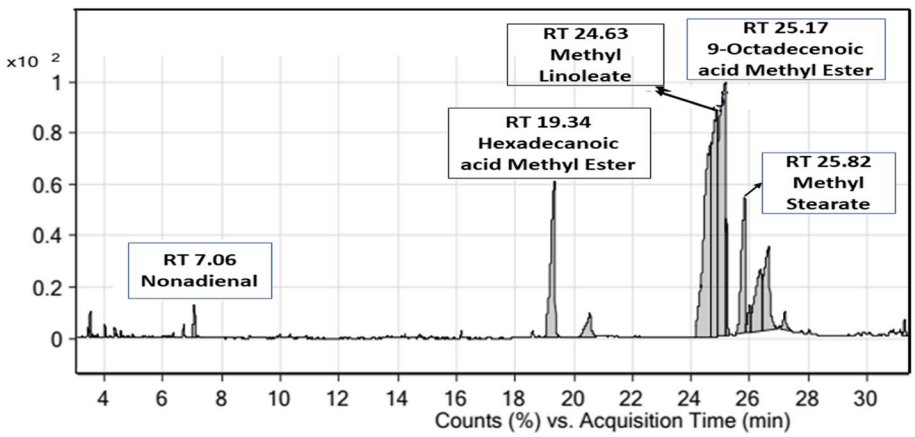

Fig. 12 GC-MS spectra of biodiesel obtained from waste cooking oil using MgO-SnO_2 nanocomposite

nanocatalyst [52]. Moreover, amount of nanocatalyst which takes part in the transesterification reaction starts to decrease since some amount of catalyst would have been lost during washing and filtration.

Analysis of composition of fatty acids using GC-MS and FTIR spectroscopy technique

Gas chromatography-mass spectrometry was carried out to identify the fatty acid methyl esters which are present in the obtained biodiesel. The peaks present in the spectrum correspond to the fatty acid methyl ester which is analyzed with the help of NIST 11 library as well as the obtained GC-MS spectra (Fig. 12). The highest peak shows the presence of 9-octadecenoic acid methyl ester with a retention time of 25.17.

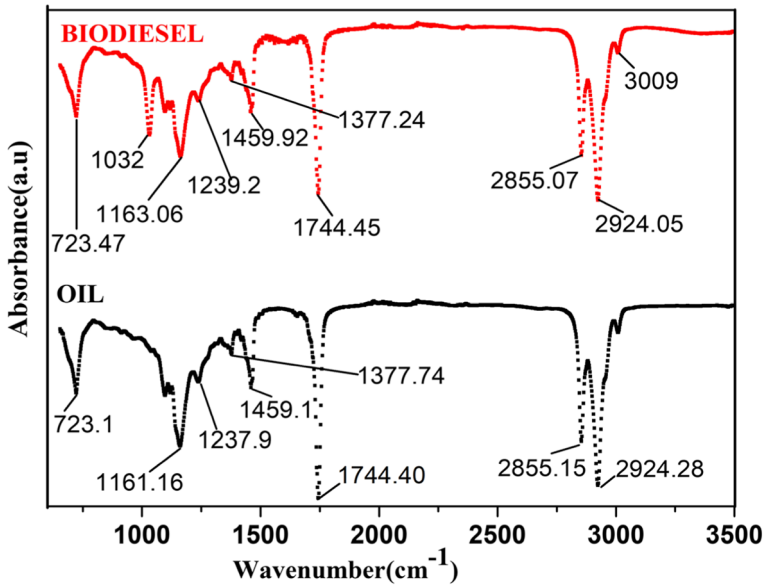

Fig. 13 FTIR spectra of biodiesel and WCO

Fourier-transform infrared spectroscopy (FTIR) was used as an analytical technique for the confirmation of fatty acid methyl ester groups. FTIR spectrum for WCO and biodiesel is given in Fig. 13. There is no absorption band seen at 3000–3500 cm^{-1} in both waste cooking oil and biodiesel, which is due to the axial deformation of −OH groups. This indicates that there is no water molecule or unreacted methanol left in both oil and biodiesel samples. The peaks at 2924.05 cm^{-1} and 2855.07 cm^{-1} are due to the stretching vibrations of symmetric and asymmetric aliphatic C–H in the CH_2 and the terminal CH_3 groups. The sharp peak seen at 1744.45 cm^{-1} is due to the carbonyl groups (C=O) stretching vibration, showing the presence of esters in the form of glycerol ester in WCO and methyl esters in biodiesel [53]. The region varying from 900 to 1500 cm^{-1} acts as the fingerprint region which is helpful to differentiate between WCO and biodiesel spectrum. The peaks due to bending vibrations of CH_3, CH_2, and $(CH_2)_n$ are at 1377.74 cm^{-1}, 1459.1 cm^{-1}, and 723.13 cm^{-1} for waste cooking oil has shifted to 1377.24 cm^{-1}, 1459.92 cm^{-1}, and 723.47 cm^{-1} for biodiesel. The peak at 1032 cm^{-1} is due to the stretching vibrations of C–O from ester which confirms the conversion of WCO into biodiesel which is absent in the waste cooking oil spectra [48].

Kinetics of biodiesel production

The pseudo-first-order and second-order rate equation are found out using the Eqs. 4 and 5.

$$\ln(1 - X) = -Kt \tag{4}$$

$$\frac{X}{1 - X} = C_{TG}Kt \tag{5}$$

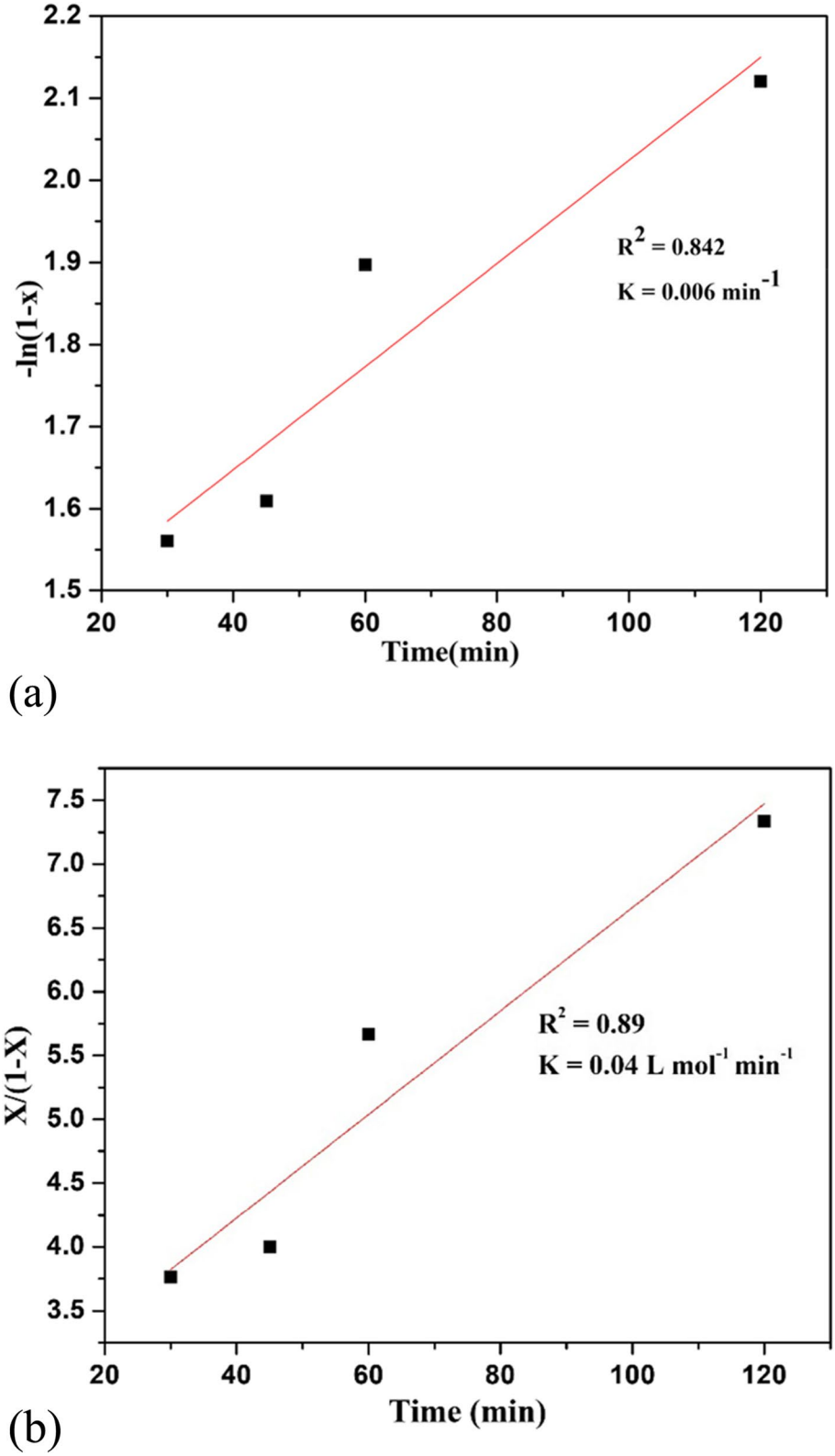

Fig. 14 **a** Pseudo-first-order rate equation plotted between −ln(1-X) versus time. **b** Pseudo-second-order rate equation plotted between X/(1-X) vs time

where X denotes the conversion of triglyceride in %, t is the reaction time in min, C_{TG} is the initial triglyceride molar concentration (mol L^{-1}), and K is rate constant of the reaction in min^{-1}.

The graph is plotted between −ln(1-X) versus time gives the pseudo-first-order rate constant value, and it is shown in Fig. 14a, whereas Fig. 14b is plotted between X/1-X versus time gives the pseudo-second-order rate constant value.

The kinetics of the transesterification reaction was carried out under optimum conditions of 18:1 methanol to oil molar ratio, 2 wt % of MgO-SnO_2 nanocomposite at a reaction temperature of 60 °C in a duration of 2 h. The kinetic model is examined with the help of the regression value coefficient R^2 which is obtained from the graphs of pseudo-first order and pseudo second order. R^2 value for pseudo-first-order rate equation is 0.842, and rate constant is found out to be 0.006 min^{-1}. R^2 value for pseudo-second-order rate equation is 0.89, and rate constant is found out to be 0.04 L mol^{-1} min^{-1}. However, as transesterification is a forward reaction, pseudo-first-order reaction is most probable.

Conclusions

MgO-SnO_2 nanocomposites were synthesized by thermal decomposition followed by sol-gel method with calcination at 600 °C for a duration of 2 h. Elemental analysis of MgO-SnO_2 nanocomposites shows the presence of Mg, O, and Sn free from other impurities which is also confirmed with the help of XPS survey. The optical energy bandgap of the nanocomposite both MgO and SnO_2 was 3 eV and 5.2 eV, respectively. The nanocomposites with size ~28 nm show increased surface area of 31.6 m^2/g, pore size of 23.9 nm, and pore volume of 0.19 mL/g. The enhanced surface properties and defect bands of the nanocomposites make them potential for applications in field optoelectronics, catalysis, and water purification. Due to this enhanced surface area and porosity of MgO-SnO_2 nanocomposite, we were able to achieve biodiesel yield of 85% using WCO as the feedstock in a duration of 60 min and highest yield of 88% in 120 min with 18:1 methanol to oil molar ratio, 2 wt% of nanocatalyst, and 60 °C of reaction temperature. Pseudo-first-order reaction tends to satisfy the kinetics model of the transesterification reaction, and rate constant was obtained as 0.006 min^{-1}. The conversion of WCO into biodiesel is confirmed with the help of FTIR and GC-MS spectra. The catalyst remains stable for repeated cycles, and conversion efficiency is slightly affected ~3%. MgO-SnO_2 nanocomposite can be used to produce biodiesel from WCO as feedstock in industrial scale.

Abbreviations

WCO	Waste cooking oil
MgO	Magnesium oxide
SnO_2	Tin oxide
MgO-SnO_2	Magnesium oxide-tin oxide
GC-MS	Gas chromatography-mass spectroscopy
FTIR	Fourier-transform infrared spectroscopy
EDS	Energy-dispersive X-ray spectroscopy
SiO_2	Silica
Co_2O_3	Cobalt (III) oxide
Al_2O_3	Alumina
TiO_2-ZnO	Titanium dioxide-zinc oxide
CaO-MgO	Calcium oxide-magnesium oxide
TiO_2-RGO	Titanium dioxide-reduced graphene oxide
WSA/ZnO/K_2CO_3	Walnut shell ash/zinc oxide/potassium carbonate

DNPH	2,4-Dinitrophenylhydrazine
BET	Brunauer–Emmett–Teller
XRD	X-ray diffraction
XPS	X-ray photoelectron spectroscopy
$SnCl_2$	Tin chloride
JCPDS	Joint Committee of the Powder Diffraction Standard
HRTEM	High-resolution transmission electron microscopy
KOH	Potassium oxide
NIST	National Institute of Standards and Technology
SAED	Selected Area (electron) Diffraction
C_2H_5OH	Ethanol
CH_3OH	Methanol
$Mg(CH_3COO)_2{\cdot}4H_2O$	Magnesium acetate tetrahydrate
$C_2H_2O_4{\cdot}2H_2O$	Oxalic acid dihydrate
$C_2H_4O_2$	Oxalic acid
RT	Retention time

Acknowledgements
We acknowledge the Academy of Maritime Education and Training for providing us the startup grant for carrying out this work.

Authors' contributions
VA has carried out the experimental part, data collection, and analysis. ARW has been responsible for concept development, design, and analysis. The author(s) read and approved the final manuscript.

Funding
No funding was obtained for this study.

Availability of data and materials
Not applicable.

Declarations

Competing interests
The authors declare that they have no competing interests.

Received: 9 June 2022 Accepted: 13 September 2022
Published online: 20 October 2022

References

1. Dahnuma D, Tasumb SO, Triwahyunia E, Nurdinb M, Abimanyua H (2015) Comparison of SHF and SSF processes using enzyme and dry yeast for optimization of bioethanol production from empty fruit bunch. Energy Proc 68:107–116
2. Shamsuddin AH (2012) Development of renewable energy in Malaysia strategic initiatives for carbon reduction in the power generation sector. Proc Eng 49:384–391
3. Feyzi M, Hosseini N, Yaghobi N, Ezzati R (2017) Preparation, characterization, kinetic and thermodynamic studies of $MgO\text{-}La_2O_3$ nanocatalysts for biodiesel production from sunflower oil. Chem Physics Lett. 677:19–29
4. Baskar G, Soumiya S (2016) Production of biodiesel from castor oil using iron (II) doped zinc oxide nanocatalyst. Renew Energy. 98:101–107
5. Kulkarni MG, Dalai AK (2006) Waste cooking oil an economical source for biodiesel: a review. Ind Eng Chem Res. 45(9):2901–2913
6. Emil A, Narayanan B, Zahira Y, Kartom KS, Salimon J (2009) Preparation of Na doped SiO_2 solid catalysts by the sol-gel method for the production of biodiesel from Jatropha oil. Green Chem. 11(11):1862–1866
7. Chakraborty R, Bepari S, Banerjee A (2011) Application of calcined waste fish (Labeo rohita) scale as low-cost heterogeneous catalyst for biodiesel synthesis. Bioresour Technol 102(3):3610–3618
8. Nizami A, Rehan M (2018) Towards nanotechnology-based biofuel industry. Biofuel Res J. 5(2):798–799
9. Refaat AA (2011) Biodiesel production using solid metal oxide catalysts. Int J Environ Sci Technol. 8:203–221
10. Sahani S, Roy T, Sharma YC (2020) Studies on fast and green biodiesel production from an indigenous nonedible Indian feedstock using single phase strontium titanate catalyst. Energy Convers Manag. 203:112180
11. Schreier M, Heroguel F, Steier L, Ahmad S, Luterbacher JS, Mayer MT, Luo J, Gratzel M (2017) Solar conversion of CO_2 to CO using earth-abundant electrocatalysts prepared by atomic layer modification of CuO. Nature Energy. 2(7):17087
12. Justine M, Joy Prabu H, Johnson I, Magimai Antoni Raj D, John Sundaram S, Kaviyarasu K (2020) Synthesis and characterizations studies of ZnO and $ZnO\text{-}SiO_2$ nanocomposite for biodiesel applications. Mater Today Proceedings. 36(2):440–446
13. Li K-T, Wang C-K, Wang I, Wang C-M (2011) Esterification of lactic acid over $TiO_2\text{-}ZrO_2$ catalysts. Appl Catalysis A General. 392(1-2):180–183

14. Nabihah-Fauzi N, Asikin-Mijan N, Ibrahim ML, Hashim H, Yusup S, Taufiq-Yap YH, Mastuli MS (2020) Sulfonated SnO_2 nanocatalysts via a self-propagating combustion method for esterification of palm fatty acid distillate. RSC Adv. 10(49):29187–29201
15. Das S, Jayaraman V (2014) SnO_2: a comprehensive review on structures and gas sensors. Prog Mater Sci. 66:112–255
16. Gurusamy S, Kulanthaisamy MR, Hari DG, Veleeswaran A, Thulasinathan B, Muthuramalingam JB, Alagarsamy A (2019) Environmental friendly synthesis of TiO_2-ZnO nanocomposite catalyst and silver nanomaterilas for the enhanced the production of biodiesel from Ulva lactuca seaweed and potential antimicrobial properties against the microbial pathogens. J Photochem Photobiol B Biol. 193:118–130
17. Shaban M, Abukhadra MR, Hosny R, Rabie AM, Ahmed SA, Negm NA (2019) Diatomite supported by CaO/MgO nanocomposite as heterogeneous catalyst for biodiesel production from waste cooking oil. J Mol Liquids. 279:224–231
18. Kuniyil M, Shanmukha Kumar JV, Adil SF, Assal ME, Shaik MR, Khan M, Al-Warthan A, Siddiqui MRH (2021) Production of biodiesel from waste cooking oil using ZnCuO/N-doped graphene nanocomposite as an efficient heterogeneous catalyst. Arab J Chem. 14:102982
19. Yusuff AS, Gbadamosi AO, Popoola LT (2021) Biodiesel production from transesterified waste cooking oil by zinc-modified anthill catalyst: parametric optimization and biodiesel properties improvement. J Environ Chem Eng. 9:104955
20. Borah MJ, Devi A, Saikia RA, Deka D (2018) Biodiesel production from waste cooking oil catalyzed by in-situ decorated TiO_2 on reduced graphene oxide nanocomposite. Energy. 158:881–889
21. Foroutan R, Peighambardoust SJ, Mohammadi R, Peighambardoust SH, Ramavandi B (2022) Application of walnut shell ash/ZnO/K_2CO_3 as a new composite catalyst for biodiesel generation from Moringa oleifera oil. Fuel. 311:122624
22. Bayal N, Jeevanandam P (2013) Sol-gel synthesis of SnO_2-MgO nanoparticles and their photocatalytic activity towards methylene blue degradation. Mater Res Bull. 48(10):3790–3799
23. Perveen H, Farrukh MA, Khaleeq-ur-Rahman M, Munir B, Tahir MA (2014) Synthesis, structural properties and catalytic activity of MgO-SnO_2 nanocatalysts. Russ J Phys Chem A. 89(1):99–107
24. Hassan HMA, Alhumaimess MS, Alsohaimi IH, Essawy AA, Hussein MF, Alshammari HM, Aldosari OF (2020) Biogenic-mediated synthesis of the Cs_2O-MgO/MPC nanocomposite for biodiesel production from olive oil. ACS Omega. 5(4):27811–27822
25. Varala R, Narayana V, Kulakarni SR, Khan M, Alwarthan A, Adil SF (2016) Sulfated tin oxide (STO) – structural properties and application in catalysis: a review. Arab J Chem. 9(4):550–573
26. Amirthavalli V, Warrier AR (2019) Production of biodiesel from waste cooking oil using MgO nanocatalyst. In: AIP Conference Proceedings, vol 2115, p 030609
27. Maimoonah Khalid Qasim (2019) Modified nanostructure MgO superbasicity with CaO in heterogenous transesterification of sunflower oil. Egyptian J Chem. 62(3):475–485
28. Zhang S-G, Yin S-F, Wei Y-D, Luo S-L, Chak-Tong A (2012) Novel MgO–SnO_2 solid superbase as a high-efficiency catalyst for one-pot solvent-free synthesis of polyfunctionalized 4H-pyran derivatives. Appl Catalysis A. 142(5):608–614
29. Essien ER, Atasie VN, Okeafor AO, Nwude DO (2019) Biogenic synthesis of magnesium oxide nanoparticles using Manihot esculenta (Crantz) leaf extract. Intern Nano Lett. 10(1):43–48
30. Chen S, Sun Z, Zhang L, Xie H (2020) Photodegradation of gas phase benzene by SnO_2 nanoparticles by direct hole oxidation mechanism. Catalysts. 10(1):117
31. Mohandes F, Davar F, Salavati-Niasari M (2010) Magnesium oxide nanocrystals via thermal decomposition of magnesium oxalate. J Physics Chem Solids. 71(12):1623–1628
32. Yang H, Yue-hua H, Tang A, Jin S, Qiu G (2004) Synthesis of tin oxide nanoparticles by mechanochemical reaction. J Alloys Compd. 363(1-2):271
33. Jiang W, Hua X, Han Q, Yang X, Lu L, Wang X (2009) Preparation of lamellar magnesium hydroxide nanoparticles via precipitation method. Powder Technol. 191:227–230
34. Umaralikhan L, Jamal Mohamed Jaffar M (2016) Green synthesis of MgO nanoparticles and its antibacterial activity. Iranian J Sci Technol Trans A Sci. 42(2):477–485
35. Seyama H, Soma M (1984) X-ray photoelectron spectroscopic study of montmorillonite containing exchangeable divalent cations. J Chem Soc Faraday Trans 1: Phys Chem Condens Ph. 80(1):237–248
36. Wagner CD, Riggs WM, Davies LE, Moulder JF, Muilenberg GE (1979) Handbook of X-ray photoelectron spectroscopy. PerkinElmer, Eden Prairie, pp 1–190
37. Song GL (2011) Corrosion of magnesium alloys. Elsevier
38. Meng D, Liu DY, Wang GS, Shen YB, San XG, Li M, Meng FL (2018) Low-temperature formaldehyde gas sensors based on NiO-SnO_2 heterojunction microflowers assembled by thin porous nanosheets. Sens Actuators B Chem. 273:418–428
39. He J, Jiao W, Zhang L, Feng R (2018) Preparation and gas-sensing performance of SnO_2/NiO composite oxide synthesized by microwave-assisted liquid phase deposition. Particuology 41:118–125
40. Bai S, Liu J, Guo J, Luo R, Li D, Song Y, Liu CC, Chen A (2017) Facile preparation of SnO_2/NiO composites and enhancement of sensing performance to NO_2. Sens Actuators B Chem. 249:22–29
41. Meng Y-L, Wang B-Y, Shu-FenLi S-JT, Zhang M-H (2013) Effect of calcination temperature on the activity of solid Ca/Al composite oxide-based alkaline catalyst for biodiesel production. Bioresour Technol. 128:305–309
42. Tang Y, Xu J, Zhang J, Lu Y (2013) Biodiesel production from vegetable oil by using modified CaO as solid basic catalysts. J Clean Prod. 42:198–203
43. Ayetor GK, Sunnu A, Joseph Parbey A (2015) Effect of biodiesel production parameters on viscosity and yield of methyl esters: Jatropha curcas, Elaeisguineensis and Cocos nucifera. Alex Eng J. 54:1285–1290
44. Yin X, Ma H, You Q, Wang Z, Chang J (2012) Comparison of four different enhancing methods for preparing biodiesel through transesterification of sunflower oil. Appl Energy. 91(1):320–325
45. Fan M, Liu Y, Zhang P, Jiang P (2016) Blocky shapes Ca-Mg mixed oxides as a water-resistant catalyst for effective synthesis of biodiesel by transesterification. Fuel Process Techno. 149:163–168

46. Amani H, Ahmad Z, Asif M, Hameed BH (2014) Transesterification of waste cooking palm oil by MnZr with supported alumina as a potential heterogeneous catalyst. J Ind Eng Chem. 20:4437–4442
47. Kawentar WA, Budiman A (2013) Synthesis of biodiesel from second-used cooking oil. Physics Proc. 32:190–199
48. Abdullah RN, Sianipar R, Ariyani D, Nata IF (2017) Conversion of palm oil sludge to biodiesel using alum and KOH as catalysts. Sustain Environ Res. 27(6):291–295
49. Hoque ME, Singh A, Chuan YL (2011) Biodiesel from low-cost feedstocks: the effects of process parameters on the biodiesel yield. Biomass Bioenergy. 35(4):1582–1587
50. AbuKhadra MR, Basyouny MG, El-Sherbeeny AM, El-Meligy MA, Abd Elatty E, Elgawad A (2020) Transesterification of commercial waste cooking oil into biodiesel over innovative alkali trapped zeolite nanocomposite as green and environmental catalysts. Sustain Chem Pharmcy. 17:100289
51. Degfie TA, Mamo TT, Mekonnen YS (2019) Optimized biodiesel production from waste cooking oil (WCO) using calcium oxide (CaO) nano-catalyst. Sci Rep. 9(1):1892
52. Foroutan R, Mohammadi R, Esmaeili H, Mirzaee Bektashi F, Tamjidi S (2020) Transesterification of waste edible oils to biodiesel using calcium oxide@magnesium oxide nanocatalyst. Waste Manag 105:373–383
53. Fadhil AB, Al-Tikrity ETB, Albadree MA (2015) Transesterification of a novel feedstock, Cyprinus carpio fish oil: influence of co-solvent and characterization of biodiesel. Fuel. 162:215–223

Publisher's Note